Pathways and Rate Coefficients for the Decomposition of Vinoxy and Acetyl Radicals

ARTICLE *in* THE JOURNAL OF PHYSICAL CHEMISTRY A · JUNE 2006

Impact Factor: 2.69 · DOI: 10.1021/jp054934r · Source: PubMed

Pathways and Rate Coefficients for the Decomposition of Vinoxy and Acetyl Radicals

Juan P. Senosiain,*,† Stephen J. Klippenstein,‡ and James A. Miller*,†

Combustion Research Facility, Sandia National Laboratories, Livermore, California 94551-0969 MS 9055, and Chemistry Division, Argonne National Laboratory, Argonne, IL 60439.

Received: August 31, 2005; In Final Form: January 25, 2006

The potential in the vicinity of the stationary points on the surface for the decomposition of ground-state vinoxy and acetyl radicals has been calculated using the RQCISD(T) method extrapolated to the infinite-basis set limit. Rate coefficients for the decomposition pathways of these two radicals were computed using the master equation and variational transition state theory. Agreement between our calculated rate coefficients for $H + CH_2CO \leftrightarrow CH_3 + CO$ and experimental data is very good, without the need for empirical adjustments to the ab initio energy barriers. Multireference configuration−interaction calculations indicate two competitive channels for vinoxy decomposition, with the channel leading to $H + CH_2CO$ being preferred at photodissociation energies. However, at typical combustion conditions, vinoxy decomposes primarily to CO and methyl. In contrast, decomposition of acetyl shows only one decomposition channel, leading to CO and methyl. The implications of a low-lying exit channel for the calculation of theoretical rate coefficients are discussed briefly.

Introduction

Vinoxy and acetyl radicals are important intermediates in combustion processes. In hydrocarbon flames, vinoxy radicals can be produced from the reactions of O (^{3}P) atoms with ethylene or terminal alkenes and the reactions of vinyl with O_2 or OH. Acetyl radicals are primarily formed by hydrogen abstraction from acetaldehyde. Such reactions are important in combustion[1,2] and interstellar chemistry.[3]

Ground-state vinoxy radicals can be described by two Lewis structures, corresponding to vinoxy, $CH_2{=}CHO\bullet$, and the formyl methyl radical, $\bullet CH_2CH{=}O$. Previous microwave spectroscopy studies revealed that electron-spin density is greatest on the methylene carbon, indicating that the latter structure is dominant.[4] Nonetheless, throughout this paper we shall use the term "vinoxy" to refer to both structures, because this name is pervasive in the literature. Vinoxy radicals have been the subject of a number of spectroscopic,[4−12] photodissociation,[13−15] and theoretical studies.[16−19] Colket et al.[20] estimated its decomposition rate coefficient by analogy with the dissociation of ethyl radicals on the basis of Benson's thermochemical kinetics principles. However, to the best of our knowledge, the only study of the thermal dissociation kinetics of vinoxy radicals is that by Lee and Bozzelli,[19] who used QRRK and RRKM methods to obtain rate coefficients for the recombination of H with ketene and the reverse reaction.

Besides the lack of experimental data for thermal decomposition, there is currently a discrepancy concerning the dissociation pathways of vinoxy radicals. Osborn et al.[13] performed fast-beam, photofragment translational spectroscopy and reported a ratio of 4(±2):1 of ketene to methyl products. In a subsequent theoretical paper,[18] Matsika and Yarkony described several conical intersections between the $\tilde{X}(^2A'')$, $\tilde{A}(^2A')$ and $\tilde{B}(^2A'')$ surfaces, but they did not elaborate on the mechanisms of internal conversion between $\tilde{X}$ and $\tilde{A}$ states. In a more recent study, Butler et al.[15] produced ground-state vinoxy directly from the photolysis of chloroacetaldehyde, and they did not detect the ketene channel in the decomposition of this radical. They attributed the absence of ketene to a preclusion of this channel caused by nonadiabatic recrossings near the transition state.

The formation and decomposition kinetics of acetyl radicals have been studied experimentally by a number of groups.[21−27] In contrast to that of H atoms with ketene, the recombination reaction of CO with methyl radicals exhibits significant pressure dependence. This led several studies to underestimate the high-pressure-limit rate coefficient. The theoretical study of Bencsura et al.[27] highlighted the importance of weak-collisional effects on this system.

The dissociation of vinoxy is a particularly complex example of a multichannel dissociation,[28] one in which there is a potential well between the reactants and one set of products. Acetyl is a very weakly bound free radical; the dissociation of such radicals exhibits a number of interesting freatures.[29] In this paper we use high-level quantum chemistry methods to calculate saddle-points and minima for the isomerization and dissociation reactions of vinoxy and acetyl radicals. We use variational RRKM theory to calculate rate coefficients as a function of energy and angular momentum quantum number and employ a master equation model to obtain rate coefficients over a broad range of temperatures and pressures. Finally, we provide statistical fitting parameters for use in chemical kinetic models.

I. Quantum Chemistry and the C_2H_3O Potential Energy Surface

To calculate the rate coefficients using variational transition state theory, the energies, optimized geometries, vibrational frequencies, and internal-rotation potentials have to be obtained for saddlepoints and stable complexes, as well as for several

* To whom correspondence should be addressed. Email: jpsenos@sandia.gov; Phone: +1 925 2942305; Fax: +1 925 2942276; Address: P.O. Box 969 M. S. 9055, Livermore, CA 94551-0969.

† Sandia National Laboratories.

‡ Argonne National Laboratory.

10.1021/jp054934r CCC: $33.50
Published on Web 04/04/2006 PAGE EST: 9.2

TABLE 1: Rovibrational Properties[a] of Isomers and Bimolecular Products

species	symm	rotational constants (cm^{-1})			σ_{rot}[b]	m[c]	frequencies[d] (cm^{-1})											
Isomers																		
CH_3CO (**1**)	$^2A'$	2.77	0.33	0.31	3	1	*104*	477	869	962	1068	1381	1480	1483	1906	3057	3153	3156
CH_2CHO (**2**)	$^2A''$	2.22	0.38	0.32	2	1	*421*	507	684	963	977	1161	1417	1491	1576	3005	3168	3287
CH_2CHO (**2′**)	$^2A'$	2.39	0.37	0.32	2	1	412	440	725	936	969	1100	1284	1451	1667	3104	3195	3298
HOCHCH	$^2A'$	2.59	0.36	0.32	1	1	*403*	484	598	817	822	1126	1267	1382	1685	3162	3313	3876
$HOCCH_2$	^2A	3.43	0.33	0.31	1	2	*344*	449	645	820	970	1142	1266	1429	1730	3139	3266	3881
$H(COC)H_2$	^2A	0.99	0.79	0.50	1	2	801	821	961	1067	1092	1147	1203	1362	1549	3137	3181	3234
Bimolecular Products																		
C_2H_2	$^1\Sigma_g^+$	1.17	1.17		2	1	534	534	769	769	2017	3436	3534					
OH	$^2\Pi$	18.85	18.85		1	1	3774											
C_2H	$^2\Sigma^+$	1.45	1.45		1	1	460	460	2038	3482								
H_2O	$^1A_1$	26.83	14.73	9.51	1	1	1654	3889	3992									
HCCOH	$^1A'$	22.08	0.32	0.32	1	1	*364*	374	551	639	1075	1295	2265	3508	3880			
H	$^2S_{1/2}$																	
HCCO	$^2A''$	32.75	0.36	0.36	1	1	483	492	547	1234	2071	3347						
H_2	$^1\Sigma_g^+$	60.52	60.52		2	1	4420											
CH_2CO	$^1A_1$	9.39	0.34	0.33	2	1	446	486	579	1003	1162	1431	2208	3215	3322			
H	$^2S_{1/2}$																	
CO	$^1\Sigma^+$	1.91	1.91		1	1	2179											
CH_3	$^2A_2''$	9.50	9.50	4.75	6	1	463	1435	1435	3126	3308	3308						

[a] Calculated at the UQCISD/6-311++G(d,p) level. [b] Rotational symmetry number. [c] Number of optical isomers, adjusted for cases with internal rotors. [d] Frequencies treated as internal rotors shown in italics.

TABLE 2: Rovibrational Properties[a] of Saddlepoints

TS	symm	rotational constants (cm^{-1})			σ_{rot}[b]	m[c]	frequencies[d] (cm^{-1})											
2 ↔ HOCHCH	^2A	1.79	0.46	0.36	1	2	2009 i	187	829	946	1045	1110	1181	1334	1451	2079	3147	3203
2 ↔ **1**	^2A	3.39	0.34	0.32	1	2	1631 i	*425*	621	841	1037	1150	1231	1470	1869	1945	3101	3289
2 ↔ $H(COC)H_2$	^2A	1.19	0.59	0.43	1	2	1400 i	481	827	879	1051	1112	1338	1391	1518	3138	3198	3248
2′ ↔ $HOCCH_2$	^2A	3.87	0.33	0.30	1	1	2192 i	*369*	434	583	726	967	1134	1427	1701	2489	3161	3286
2 ↔ H+CH_2CO	^2A	3.39	0.34	0.32	2	1	737 i	*158*	432	485	553	613	997	1155	1435	2171	3214	3334
1 ↔ H+CH_2CO	$^2A'$	3.25	0.31	0.30	1	1	784 i	290	424	543	561	798	1029	1119	1423	2183	3199	3303
1 ↔ CO+CH_3	$^2A'$	2.00	0.25	0.23	3	1	463 i	*42*	272	531	602	930	1442	1449	2034	3103	3261	3276

[a] Calculated at the UQCISD/6-311++G(d,p) level. [b] Rotational symmetry number. [c] Number of optical isomers, adjusted for cases with internal rotors. [d] Frequencies treated as internal rotors shown in italics.

points in the vicinity of each saddlepoint along the intrinsic reaction coordinate (IRC). For this purpose, we used the 6-311++G(d,p) Gaussian basis set and spin-unrestricted hybrid density functional theory with the UB3LYP functional.[30,31] To ascertain the accuracy of these geometries and frequencies, we performed additional geometry optimizations and frequency calculations of all stationary points on the potential energy surface using the spin-unrestricted, quadratic configuration-interaction method with single and double excitations, UQCISD, and the same basis set. Table 1 shows the rovibrational properties of the C_2H_3O isomers and bimolecular channels using the latter method, and Table 2 shows these properties for the associated saddlepoints. For comparison, rovibrational properties calculated with UB3LYP are provided in the Supporting Information section. To obtain accurate energy barriers, we performed single-point energy calculations on the UB3LYP and UQCISD geometries using the RQCISD(T) method, together with Dunning's correlation-consistent basis sets. The energies were extrapolated to the infinite-basis-set limit with the asymptotic form suggested by Martin[32] and Feller and Dixon,[33]

$$E_\infty = E_{l_{max}} - B/(l_{max} + 1)^4 \quad (1)$$

where l_{max} is the maximum component of angular momentum in the cc-pVnZ basis set, and E_∞ is the infinite basis-set energy. In this case, triple- and quadruple-ζ basis sets were used, i.e., $l_{max} = \{3,4\}$. Henceforth, we denote properties obtained at the RQCISD(T)/cc-pV∞Z level and UB3LYP and UQCISD/6-311++G(d,p) geometries and vibrational frequencies simply as RQCIT//DFT and RQCIT//QCI, respectively. The related RCCSD(T) method has been shown[34] to achieve "chemical accuracy", even in situations where spin contamination would normally be a problem. However, our own unpublished calculations show that the RQCISD(T) method performs slightly better than the popular RCCSD(T) method in the calculation of a series of well-known adiabatic energy barriers.[35]

Calculated energies (including ZPE) for isomers and related transition states are tabulated in Tables 3 and 4, respectively, and shown graphically in Figure 1. Energies obtained at the RQCIT//DFT and RQCIT//QCI theoretical model chemistries are generally within 0.5 kcal/mol, except those of the saddle-point for acetyl decomposition leading to ketene, TS(**1** ↔ H + CH_2CO), where the RQCIT//QCI is 1 kcal/mol higher. We note that the variational approach sometimes compensates for the underestimation of energy barriers due to geometries optimized at lower levels of theory. For instance, the IRCmax [In a system calculated at two theoretical model chemistries, the IRCmax is the energy maximum (computed at the high-level of theory) on the IRC optimized with the lower level of theory.] at the RQCIT//DFT level for this transition state is 1.3 kcal/mol higher than the energy barrier at the same level of theory, in closer agreement with the RQCIT//QCI barrier.

The zero-point energies (ZPE) calculated with these two methods are shown in Tables 3 and 4. In general, the differences in ZPE are smaller that those of the total energies. Also shown are the Q1 diagnostics (also called T1 diagnostics in some electronic structure codes) of Lee et al.[36,37] for these structures. A Q1 diagnostic greater than 0.02 is an indication that a single determinant is insufficient to describe the wave function, suggesting multireference methods might be more suitable.

TABLE 3: Calculated Energies, Q1 Diagnostic, and Zero-point Energies of Isomers and Bimolecular Products

species	symm	calculated energy[a] (kcal mol^{-1}) QCI[b]	RQCIT//QCI[c]	RQCIT//DFT[d]	Q1 diagnostic[b]	ZPE QCI[a]	DFT[e]
Isomers							
CH_3CO (**1**)	$^2A'$	−6.6	−6.6	−6.8	0.022	27.3	27.0
CH_2CHO (**2**)	$^2A''$	0.0	0.0	0.0	0.022	26.7	26.5
CH_2CHO (**2′**)	$^2A'$	23.2	23.0	23.3	0.021	26.6	26.7
HOCHCH	$^2A'$	29.8	27.4	27.2	0.016	27.1	26.7
$HOCCH_2$	^2A	25.8	23.8	23.5	0.019	27.3	26.8
$H(COC)H_2$	^2A	38.1	36.1	35.7	0.022	28.0	27.4
Bimolecular Products							
C_2H_2	$^1\Sigma_g^+$	55.9	57.9	58.3	0.014	22.0	22.2
OH	$^2\Pi$				0.007		
C_2H	$^2\Sigma^+$	72.5	72.3	71.8	0.017	22.8	22.1
H_2O	$^1A_1$				0.007		
HCCOH	$^1A'$	71.6	68.7	68.8	0.014	19.9	19.9
H	$^2S_{1/2}$				0.000		
HCCO	$^2A''$	38.1	36.4	36.8	0.026	18.0	18.0
H_2	$^1\Sigma_g^+$				0.006		
CH_2CO	$^1A_1$	36.8	34.9	35.0	0.017	19.8	19.8
H	$^2S_{1/2}$				0.000		
CO	$^1\Sigma^+$	−2.8	2.2	2.2	0.019	21.8	21.8
CH_3	$^2A_2''$				0.006		

[a] Including zero-point vibrational energy. [b] UQCISD/6-311++G(d,p). [c] RQCISD(T) /cc-pV∞Z // UQCISD/6-311++G(d,p). See text for details. [d] RQCISD(T) /cc-pV∞Z // UB3LYP/6-311++G(d,p). See text for details. [e] UB3LYP /6-311++G(d,p).

TABLE 4: Calculated Energies[a], Q1 Diagnostic and Zero-point Energies of Saddlepoints

TS	symm	calculated energy[a] (kcal mol^{-1}) QCI[b]	RQCIT//QCI[c]	RQCIT//DFT[d]	IRCmax RQCIT//DFT[d]	QI Diagnostic[a]	ZPE QCI[a]	DFT[e]
2 ↔ HOCHCH	^2A	66.3	62.4	62.2		0.027	23.6	23.3
2 ↔ **1**	^2A	44.4	40.3	40.1		0.027	24.3	23.9
2 ↔ $H(COC)H_2$	^2A	54.6	50.4	49.9		0.049	26.0	25.7
2′ ↔ $HOCCH_2$	^2A	62.2	57.4	57.1		0.017	23.3	22.9
2 ↔ H + CH_2CO	^2A	45.7	42.5	42.1	43.1	0.025	20.8	21.0
1 ↔ H + CH_2CO	$^2A'$	42.3	39.2	38.2	39.5	0.022	21.3	20.9
1 ↔ CO + CH_3	$^2A'$	8.0	9.8	9.0	9.8	0.023	24.2	23.7

[a] Including zero-point vibrational energy. [b] UQCISD/6-311++G(d,p). [c] RQCISD(T) /cc-pV∞Z // UQCISD/6-311++G(d,p). See text for details. [d] RQCISD(T) /cc-pV∞Z // UB3LYP/6-311++G(d,p). See text for details. [e] UB3LYP /6-311++G(d,p).

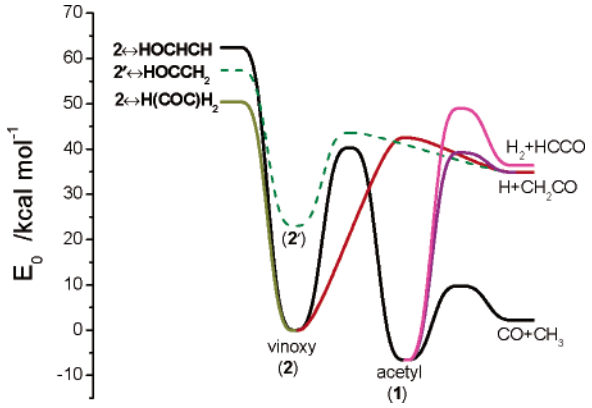

Figure 1. Simplified C_2H_3O potential energy surface using the RQCIT//QCI theoretical model chemistry (see text for details), including dissociation and isomerization channels. A second-order saddlepoint for planar dissociation of Ã vinoxy ($^2A'$) is shown with a dashed line.

Although many of the structures shown in Tables 3 and 4 have a Q1 diagnostic greater than 0.02, none are exceptionally large; thus, the error expected from the single reference method should not be too great.

To assess the effect of static correlation on the decomposition pathways of vinoxy radicals, we performed multireference configuration−interaction calculations for the dissociation and isomerization channels. Geometries were optimized with the complete active space (CAS) self-consistent field method, state averaging the lowest two states with equal weighting, using the 6-311++G(d,p) basis set. The active space for the isomerization barrier (**2** ↔ **1**) included 7 electrons and 6 orbitals, which include the σ and σ^* orbitals between the transferred hydrogen and the two carbon atoms, as well as the C−O π and π^* orbitals. The active space for the dissociation reaction (**2** ↔ H + CH_2CO) and related structures also included 7 electrons and 6 orbitals, namely the σ and σ^* orbitals of the C−H bond, and the π and π^* orbitals corresponding to the C−O and C−C bonds. The effect of dynamical correlation was taken into account by performing second-order multireference perturbation theory based on a CASSCF reference function (CASPT2) and multireference, configuration-interaction with singles and doubles and a Davidson estimate of quadruple excitations (MRCI+Q). Single-point energies were computed with the cc-pV*n*Z basis sets and extrapolated to the infinite-basis set limit, as mentioned above.

The results of the multireference configuration−interaction calculations, together with RQCISD(T) single-point energies obtained at the SA-CASSCF geometries, are shown in Table 5. We note that although the CAS energies (particularly for the isomerization barrier) are unconverged with respect to the active space used, the energies of correlated methods are not very sensitive. For example, expanding the active space to 11 electrons and 8 orbitals, the CASPT2, MRCI, and MRCI+Q energies are within 2.1, 1.1, and 0.7 kcal/mol, respectively, of those shown in Table 5. The RQCISD(T) values are expected

TABLE 5: Calculated Energies[a] for Vinoxy Decomposition

species	PG[b]	symm	CAS	CASPT2	MRCI	MRCI+Q[c]	RQCISD(T)	ref 38[d]
CH_2CHO (**2**)	Cs	$^2A''$	0	0	0	0	0	0
conical intersection	Cs	$^2A' \leftrightarrow {}^2A''$	37.7	32.6	35.7	35.0	33.5	32.8[e]
CH_2CHO (**2′**)	Cs	$^2A'$	23.6	21.9	23.9	23.6	24.0	30.8[f]
TS(**2′** ↔ H + CH_2CO)[g]	Cs	$^2A'$	60.8	44.5	52.5	50.7	49.4	
TS(**2** ↔ H + CH_2CO)	Cs	$^2A'$	53.9	45.2	50.9	50.5	49.7	50.2
H + CH_2CO	K,C_{2v}	$^2A + {}^1A_1$	45.7	38.5	42.0	41.9	41.7	44.3
TS(**2** ↔ **1**)	C1	^2A	65.0	37.8	49.8	46.1	43.1	43.8

[a] Single-point energies (not including ZPE) extrapolated to the infinite-basis set limit, obtained at SA-CASSCF/6-311++G(d,p) geometries. Units are kcal/mol. [b] Point group. [c] Including Davidson correction. [d] MRCI+Q (Pople's correction) cc-pVTZ. [e] R(CH) = 1.101 Å. MRCI energy taken from ref 18. [f] Energy at the ground-state geometry. [g] Partially constrained geometry (planar).

to be the most accurate because this method recovers the most electron correlation. However, the energies calculated with the MRCI+Q and RQCISD(T) are similar (within 1.5 kcal/mol), lending some confidence that these results are within an estimated 2 kcal/mol error.

When restricted to planar geometries, dissociation of ground state ($^2A''$) vinoxy correlates diabatically with triplet ketene, whereas the $\tilde{A}(^2A')$ state correlates with ground-state ketene. Previous calculations by Matsika and Yarkony[18] have shown that there are at least two conical intersections between the $\tilde{X}$ and $\tilde{A}$ surfaces of vinoxy. We find a conical intersection (CI) between these two states at R(CH) = 1.0913 Å, with an energy that is well below those of the isomerization and dissociation saddlepoints (cf. Table 5). Thus, we anticipate that conversion between these two states is rapid compared to the time scale of the dissociation reaction. Interestingly, the structure of TS(**2** ↔ H+CH_2CO) optimized with the UQCISD method has no symmetry, but the SA-CASSCF structure has a mirror plane (C_s, nonplanar) with the CH_2 and CHO moieties perpendicular. The study by Young and Yarkony[38] attributes the nonplanarity of this transition state to the change of hybridization of the carbon atom in the CH_2 moiety. If we constrain the reaction to be in a plane, the minimum energy pathway for dissociation of $\tilde{A}$ vinoxy to ground-state ketene goes through an energy maximum, TS(**2′** ↔ H + CH_2CO), which is a second-order saddlepoint. This structure is almost 7 kcal/mol higher than the nonplanar structure fully optimized at the CAS level. However, as correlation energy is added, the energy differences between the planar and nonplanar structures become quasi-degenerate. Although the energy of the transition state for isomerization, TS(**2** ↔ **1**), is about 4.5 kcal/mol below that for decomposition, after adding zero-point energy, the difference is significantly reduced; consequently, both of these channels are competitive for thermal decomposition.

The Gaussian98[39] package of electronic structure programs was used to perform the UB3LYP and UQCISD calculations, and Molpro[40] was used for the RQCISD(T) and all multireference calculations. All calculations were performed with a 16-processor Linux cluster.

II. Calculation of Rate Coefficients

Rate coefficients as a function of total energy and total angular momentum were calculated using RRKM theory. Internal rotors were treated using the Pitzer−Gwinn approximation,[41] using Fourier fits to the UB3LYP rotation potentials, as described elsewhere.[42] Densities of states and numbers of states were obtained with the exact counting method. Asymmetric Eckart barriers were employed to compute the effects of tunneling and nonclassical reflection through the reaction barriers.

The rate coefficients as a function of pressure and temperature were obtained by solving the total-energy resolved (i.e., 1-D) master equation (ME) for the two-well system,

$$\frac{dn_i(E)}{dt} = Z\int_{E_{0_i}}^{\infty} P(E \leftarrow E')n_i(E')dE' - Zn_i(E) - \sum_{j\neq i}^{2} k_{ji}(E)n_i(E) + \sum_{j\neq i}^{2} k_{ij}(E)n_j(E) - k_{\mathbf{P}_\alpha i}(E)n_i(E) + n_{\mathbf{R}}K_{\mathbf{R}i}^{eq}k_{\mathbf{R}i}(E)\frac{\rho_i(E)e^{-\beta E}}{Q_i(T)} - k_{\mathbf{R}i}(E)n_i(E) \quad (2)$$

where $i = \mathbf{1}$ corresponds to acetyl and $i = \mathbf{2}$ corresponds to vinoxy radicals, **R** corresponds to the reactants (H + CH_2CO), and $\mathbf{P}_\alpha$ corresponds to a set of bimolecular products or a stable complex whose isomerization is treated irreversibly. The term involving $k_{ji}(E)$ represents the rate of isomerization from i to j, where i and j are the stable isomers, while $K_{\mathbf{R}i}^{eq}$ is the pseudo-first-order equilibrium constant (i.e., the equilibrium constant multiplied by the concentration of the excess reactant). In eq 2, $n_i(E)$ is the population of complex i at energy E, E_{0_i} is the the ground-state energy of complex i, and Z is the collision number per unit time. Collision rates were calculated using the Lennard-Jones potential parameters of ethanol[43] to represent the complexes. $P(E \leftarrow E')$ is the probability that a complex with an energy between E' and $E' + dE'$ will be transferred by a collision to a state with an energy between E and $E + dE$. Rates of collisional energy transfer (CET) for deactivating collisions were modeled using the "single exponential down" expression:

$$P(E \leftarrow E') \propto \exp\left(-\frac{E' - E}{\langle \Delta E_d \rangle}\right), \quad E' > E \quad (3)$$

where $\langle \Delta E_d \rangle$ is an energy transfer parameter that depends on the nature of the collider gas. The value of $\langle \Delta E_d \rangle$ was determined as a function of temperature by fitting the data of Michael et al.[44] for the addition of OH to acetylene to a function with linear temperature dependence between 228 and 413 K. CET rates for activating collisions were obtained from detailed balance.

To simplify the problem, isomerizations to HOCHCH, $HOCCH_2$, and $H(COC)H_2$ were treated irreversibly, as was the dissociation to bimolecular products. Rate coefficients were extracted from the solution eigenpairs following the procedures described elsewhere.[45−47] All rate coefficients were calculated with the VARIFLEX code.[48]

The ME described in the preceding paragraphs is one-dimensional (1-D) with E, the total energy, as the single independent variable. For some special cases, we can and do solve the two-dimensional (2-D) analogue of eq 2 with both E and J, the total angular momentum quantum number, as independent variables. In obtaining rate coefficients for the H + $CH_2CO \leftrightarrow CH_3$ + CO reaction, we solve the 2-D ME in the

collisionless limit[49,50] ($Z \rightarrow 0$). This approximation is quite accurate at temperatures and pressures of interest (justified by direct computation for the 1-D ME) because of the short lifetimes of the intermediate complexes. For single-well, irreversible (multichannel) dissociations, we can also solve a 2-D ME.[29,51−53] The applicability of such a model is justified in the next paragraph.

Because the bimolecular exit channel leading to $CH_3 + CO$ (**1** ↔ $CO+CH_3$) is significantly lower in energy than the other transition states, dissociation from well **2** is decoupled. Thus, this system can be considered as two single-well problems, treating the "isomerization" irreversibly as dissociation from vinoxy to $CH_3 + CO$. This was verified by solving the 1-D ME for each of the single-well problems at several temperatures and pressures, and comparing the results with those of the 1-D ME for the two-well system. Rate coefficients for the (irreversible) decomposition of vinoxy and acetyl radicals were obtained by solving the 2-D ME[29,51−53] for each individual well as a function of temperature and pressure. Unless otherwise noted, the following results are based on the single-well, 2-D calculations.

As expected, rotational effects are significant only for dissociation reactions and are almost negligible for isomerization. For example, at 0.025 atm and 800 K, k_{2D}/k_{1D} is about 0.77 and 0.93 for the dissociation and isomerization channels of vinoxy decomposition, respectively, and $k_{2D}/k_{1D} \approx 0.85$ for acetyl decomposition. This difference is due to the larger moments of inertia of the transition states for dissociation processes compared to those for isomerization.

Variational effects were quantified employing the RQCIT//DFT theoretical model chemistry (i.e., using B3LYP geometries and frequencies). The final rate coefficients were obtained from conventional RRKM calculations based on the RQCIT//QCI surface and corrected for variational effects using the ratio of k_{VTST}/k_{TST} from the RQCIT//DFT rates at each temperature and pressure. In most cases, variational effects are not very important, less than 20%, even at high temperatures. An exception is the case of acetyl decomposition, where high-pressure variational rate coefficients are up to 40% smaller than those obtained from conventional transition-state theory with the transition state located at the saddle-point.

III. Reaction of Ketene with H Atoms

There have been a number of experimental measurements of the rate coefficient of the reaction of ketene with atomic hydrogen at low[54,55,44] and high temperatures[56,1,2]. In all of these studies, $CH_3 + CO$ was found to be the sole set of reaction products, and no appreciable pressure dependence was found. A theoretical study by Lee and Bozzelli[19] reported that the stabilization of vinoxy was important below 600 K at 1 atm, whereas the reverse reaction and isomerization to acetyl were dominant above 1000 K. We examined this reaction using the two-well master equation model described in Section II, on the basis of RQCIT//DFT and RQCIT//QCI methods. Calculated rate coefficients at the high-pressure limit (i.e., the capture rate coefficient) are shown in Figure 2 for both of these model chemistries, along with the collisionless limit for the latter model chemistry and the previous studies mentioned above.

At low temperatures, the RQCIT//DFT-derived rate coefficients underestimate the low-temperature data of Michael et al.[44] However, decreasing the barrier for addition to form acetyl (**1** ↔ $H + CH_2CO$) by 0.85 kcal/mol results in rate coefficients that are in good agreement with these data. In contrast, the RQCIT//QCI model agrees well with these measurements, with no empirical adjustments to the energy barriers. Rate coefficients

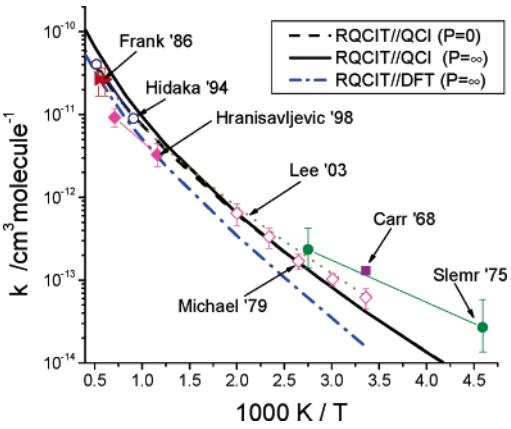

Figure 2. Bimolecular rate coefficients for the reaction of H with ketene. Rate coefficients in the high-pressure and collisionless limits were calculated with the two-well master equation method. Rate calculations are based on RQCISD(T)/cc-pV∞Z potential energy surfaces, with geometries optimized with the UQCISD and UB3LYP methods. Values reported by another theoretical study[19] are shown with a dotted line, and experimental data[1,2,44,54−56] are shown with symbols.

reported by Carr et al.[54] and Slemr and Warneck[55] are somewhat higher, e.g., by a factor of 2 at 298 K. Although the barriers resulting from these two methods are similar, the RQCIT//QCI method is probably more suitable for calculation of rate coefficients due to the improved geometries and vibrational frequencies.

At 1000 K, the difference between the high-pressure and the collisionless-limit rate coefficients becomes significant and increases with temperature. At 1500 K, $k_0/k_\infty = 57\%$, and at 2500 K this ratio decreases to about 45%. The shock-tube results of Frank et al.[56] and Hidaka et al.[1] are essentially at the collisionless limit, and agreement between these experiments and the RQCIT//QCI rate coefficients calculated at the collisionless limit is very good. However, these rate coefficients are somewhat larger than the laser-photolysis, shock-tube determinations of Michael et al.[2] between 863 and 1600 K. At 2000 K, the rate coefficients for the addition channels forming vinoxy and acetyl radicals are about equal. At this temperature, the (variational) rate coefficients at the high-pressure limit calculated with UB3LYP geometries and frequencies are about 50% smaller than those based on conventional transition state theory and UQCISD saddlepoint geometries and frequencies; the discrepancy is mostly due to the differences in frequencies. Note that the QCISD saddlepoint occurs at a C−H distance (A plot of the RQCIT//DFT potential for this reaction is provided in the Supporting Information.) of 1.91 Å, which is closer to the value of 1.82 Å for the RQCIT//DFT potential maximum (IRCmax) than that of the B3LYP saddlepoint at 2.08 Å. The energy and projected frequencies at that geometry of the RQCIT//QCI IRCmax are expected to be slightly larger than those at the saddlepoint; thus, a variational treatment should decrease the rate coefficients slightly, lessening the differences between the two methods.

Because the TS(**2** ↔ $H + CH_2CO$) is higher in energy than TS(**1** ↔ $H + CH_2CO$) by about 3.3 kcal/mol, the fraction of the reacting flux that goes through the former channel increases with temperature. For example, in the high-pressure limit, flux through TS(**2** ↔ $H + CH_2CO$) accounts for ∼14% and 31% of the total reactive flux at 1000 and 2000 K, respectively. Nonetheless, $CH_3 + CO$ are effectively the only products of this reaction, with very little vinoxy being stabilized. For instance, at 1 atm, vinoxy accounts for a maximum of 6% of the total products at temperatures in the range of 600−700 K.

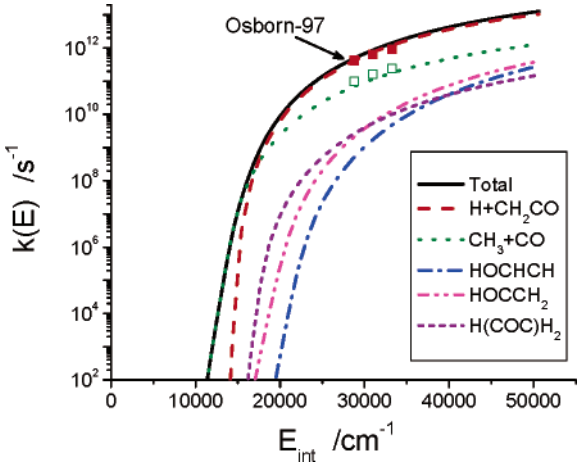

Figure 3. Calculated E-resolved rate coefficients for the decomposition pathways of vinoxy. Calculations by Osborn et al.[13] for H + CH_2CO and CO + CH_3 channels are shown with solid and open symbols, respectively.

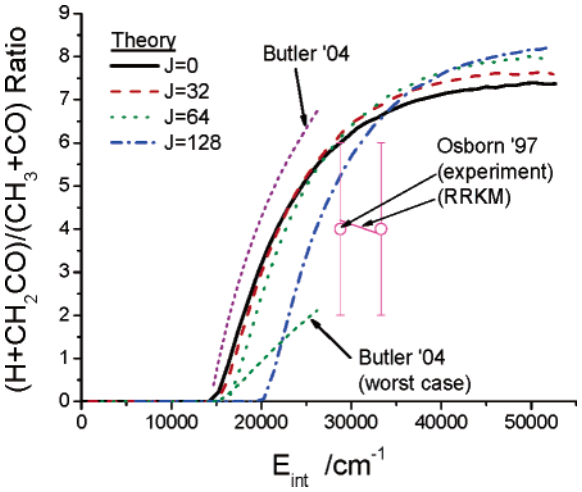

Figure 4. Ratio of rate coefficients leading to H + CH_2CO and CO + CH_3, calculated for several values of the angular momentum quantum number (lines). Experimental ratios from the work of Osborn et al.[13] are shown with symbols. Ratios from RRKM calculations of Osborn et al.[13] and Butler et al.[15] are shown with lines.

IV. Vinoxy Decomposition

Microcanonical rate coefficients, as a function of (total) internal energy, are shown in Figure 3 for the different decomposition channels of vinoxy radicals. Interestingly, we find that the CH_3 + CO channel is favored at low energies whereas the H + CH_2CO channel dominates at high energies, with the crossing point at about 50 kcal/mol of internal energy. Other transition states leading to HOCHCH, $HOCCH_2$, and cyclic $H(COC)H_2$ isomers are energetically inaccessible, even at high combustion temperatures. Our rate coefficients for the principal channels are in agreement with the RRKM calculations of Osborn et al.[13] However, the Osborn work reported a considerably smaller barrier for the ketene channel, which is contrary to the results of our calculations at all levels of theory.

The ratio of the H + CH_2CO to CH_3 + CO dissociation channels, calculated for several values of the total angular momentum, is plotted in Figure 4. The product branching ratios (Note that at photodissociation energies, this ratio is insensitive to the energy barriers and is simply given by the ratio of A-factors.) of 6−7 that we calculate at internal energies of 30 000 cm^{-1} are somewhat higher those reported by the Osborn

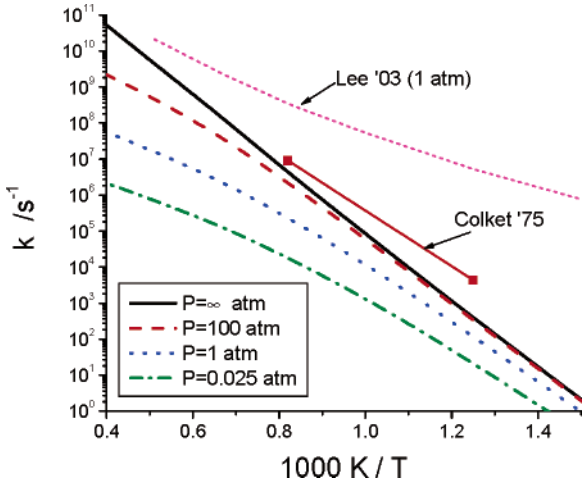

Figure 5. Calculated thermal rate coefficients for the decomposition of vinoxy radicals as a function of pressure of Ar collider bath. Also shown are results from previous studies.[19,20]

paper for experiments (4 ± 2) and RRKM calculations (∼4). They lie between those calculated by Butler et al.[15] based on a G3//B3LYP surface and those of their modified "worst case scenario" (WC). The Butler work reported that they did not observe the ketene channel, and estimated that it is suppressed by a factor of 50−200 relative to their RRKM calculations. They attributed this suppression to the nonadiabatic recrossing of dissociation pathways constrained to planar geometries and/or to slow intramolecular vibrational energy redistribution (IVR) into the torsional mode of vinoxy. Our RRKM rate coefficients are based on the assumption of strong-mode coupling; thus, no conclusion about nonstatistical effects can be drawn. However, slow IVR into the torsional mode of vinoxy is not expected, given the existence of several medium-frequency modes that differ by amounts comparable to the torsional frequency. Furthermore, the energy of the conical intersection between the $\tilde{X}(^2A'')$ and the $\tilde{A}(^2A')$ surfaces is only about 35 kcal/mol above ground-state vinoxy; thus, internal conversion is expected to be rapid compared to the time scale of the decomposition reaction. Recently, Young and Yarkony[38] analyzed the potential energy surface in the vicinity of TS(**2** ↔ H + CH_2CO) and concluded that the topologies of the conical intersections in this region are not consistent with a nonadiabatic recrossing of the transition state.

An Arrhenius plot for the thermal decomposition of vinoxy radicals is shown in Figure 5 as a function of pressure. Although H + CH_2CO is the predominant channel for photodissociation, at the lower energies corresponding to typical combustion conditions, the main channel is the decomposition to CH_3 + CO through TS(**2** ↔ **1**). Our calculations for the total rate coefficients of vinoxy dissociation are somewhat smaller than the empirical estimates of Colket et al.[20] and orders of magnitude smaller than the QRRK calculations of Lee and Bozzelli.[19]

The fraction of vinoxy that dissociates to H + ketene is shown in Figure 6. Dissociation to ketene constitutes about 34% of the total rate constant at 1000 K and 1 atm and rises to 58% at 100 atm. At 2000 K and 100 atm, the ketene channel is about 3 times faster than that leading to CH_3 + CO products.

V. Reaction of CO with Methyl Radicals

There have been a number of studies[24,25,57] reporting the high-pressure limit for the bimolecular reaction between CO and

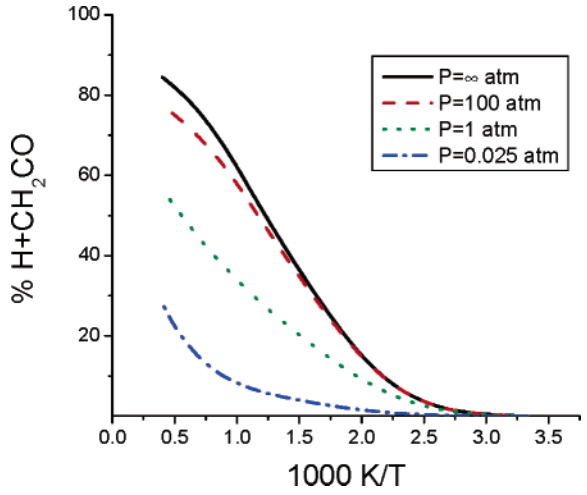

Figure 6. Fraction of the total rate coefficient for dissociation of vinoxy radicals leading to H + ketene at several pressures of Ar collider.

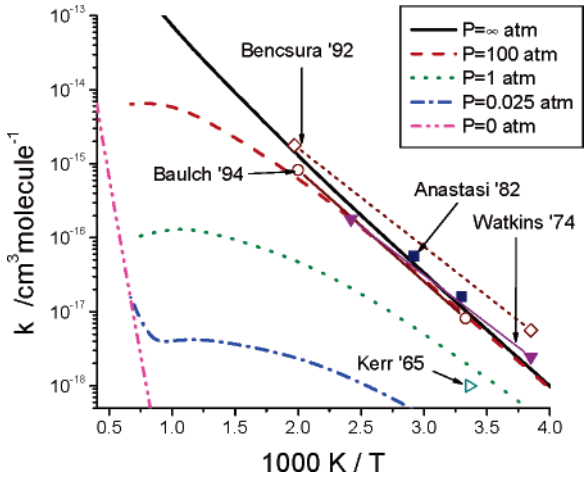

Figure 7. Bimolecular rate coefficients for the reaction of CH_3 with CO. Calculated rate coefficients from this study are based on RQCIT// QCI surface and are shown with lines. High-pressure rate coefficients from previous studies[22,24,25,27] and a literature review[58] are shown with symbols.

methyl radicals, all of these below 500 K. These data, along with our calculations at several pressures of Ar collider are shown in Figure 7. This reaction exhibits a strong pressure dependence, even below room temperatures. Comparison between our calculations and the results of Anastasi and Maw,[25] Watkins and Word,[24] and the literature review of Baulch[58] is quite favorable. These measurements lie somewhat lower than the TST model of Bencsura et al.[27] at low temperatures, but agreement between our results and theirs is generally good. However, earlier work by Kerr and Calvert[22] resulted in noticeably smaller rate coefficients, possibly due to the fact that they used a simple Lindemann−Hinshelwood model to extrapolate to the high-pressure limit.

VI. Acetyl Decomposition

At thermal energies, acetyl radical decomposes exclusively to CO + CH_3, because all other channels have significantly higher energy barriers. This is evident in Figure 8, which shows the microcanonical rate coefficients for each channel. Thermal rate coefficients calculated for several pressures of Ar bath gas are shown in Figure 9, together with several experimental determinations reportedly in the high-pressure limit[21−23,26,27] and

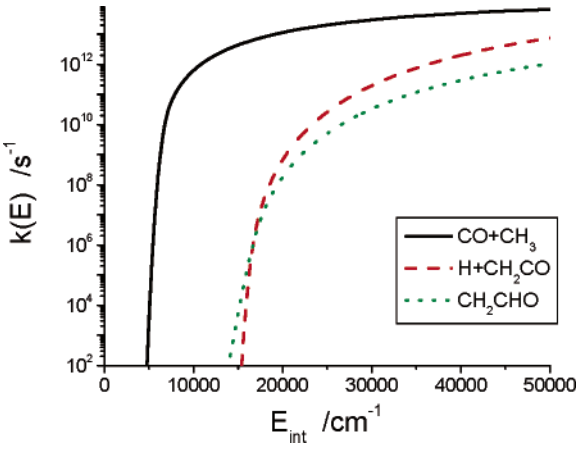

Figure 8. Calculated E-resolved rate coefficients for the decomposition pathways of acetyl radical.

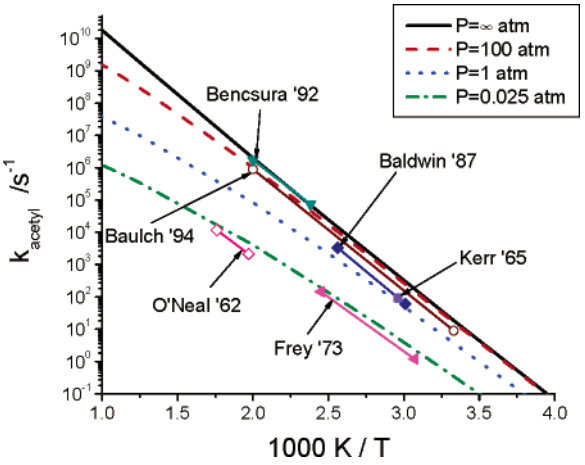

Figure 9. Thermal rate coefficients for decomposition of acetyl radicals calculated at several pressures of an Ar collider gas. Data from previous studies[21−23,26,27] and a literature review[58] shown with symbols.

the literature evaluation by Baulch et al.[58] Agreement between our calculations and the rate coefficients of Baldwin et al.[26] and Baulch's recommendation is very good. Early work[21,23] show unusually small A-factors, possibly caused by ignoring weak collision effects in the extrapolation to the high-pressure limit.

Decomposition of acetyl radicals is very great compared with that of vinoxy radicals. The relatively low dissociation threshold for acetyl decomposition poses a number of complications for the theoretical analysis. The typical RRKM/ME approach relies on the separation of time scales,

$$\tau_{IVR} \ll \tau_{CET} \ll \tau_{chem} \quad (4)$$

where τ_{IVR}, τ_{CET}, and τ_{chem} are the characteristic times for intramolecular vibrational relaxation, collisional energy transfer, and chemical reaction, respectively. At high internal energies, such as those resulting from chemical activation, the dissociation rates through a low-energy channel can be so fast that they approach those of CET or IVR processes. Such is the case for acetyl decomposition, where several studies have shown that at high energies this reaction exhibits non-statistical behavior[14,59] (i.e., non-RRKM). However, usually before this happens, chemical reactions can interfere with the CET process that is trying to establish a Maxwellian energy distribution.

TABLE 6: Fitting Parameters[a] for Calculated Rate Coefficients

reaction	*P*/atm[b]	*A*	*B*	*C*
$CH_2CHO \rightarrow H + CH_2CO$	∞	1.43×10^{15}	−0.15	22952
	100	1.18×10^{36}	−6.48	27766
	10	3.46×10^{36}	−6.92	26663
	1	1.32×10^{34}	−6.57	24889
	0.1	2.37×10^{30}	−5.86	23208
	0.025	2.48×10^{27}	−5.23	22297
	0.01	2.39×10^{25}	−4.80	21854
$CH_2CHO \rightarrow CH_3 + CO$	∞	2.93×10^{12}	0.29	20295
	100	2.23×10^{33}	−5.97	25389
	10	2.15×10^{35}	−6.76	24936
	1	6.51×10^{34}	−6.87	23750
	0.1	6.37×10^{32}	−6.57	22286
	0.025	1.54×10^{31}	−6.27	21378
	0.01	1.16×10^{30}	−6.07	20801
$CH_3CO \rightarrow CH_3 + CO$	∞	1.07×10^{12}	0.63	8503
	100	1.26×10^{20}	−2.32	9065
	10	8.18×10^{19}	−2.55	8688
	1	6.45×10^{18}	−2.52	8272
	0.1	1.96×10^{16}	−2.09	7648
	0.025	2.40×10^{15}	−2.00	7451
	0.01	6.88×10^{14}	−1.97	7340
$H+CH_2CO \rightarrow CH_3CO$	∞	3.82×10^{-16}	1.61	1322
$H+CH_2CO \rightarrow CH_2CHO$	∞	3.30×10^{-15}	1.43	3045
$H+CH_2CO \rightarrow CH_3 + CO$	0	1.29×10^{-15}	1.45	1399

		A	*B*	*C*	*D*	*E*	*F*
$CH_3 + CO \rightarrow CH_3CO$	∞	3.64×10^{-15}	0.98	5020	1.03×10^{-14}	0.71	3294
	100	7.45×10^{15}	3.67	245753	2.17×10^{-3}	−3.23	4395
	10	1.51×10^{-21}	2.83	17591	2.50×10^{-1}	−4.17	4356
	1	7.64×10^{-25}	3.67	14998	6.13×10^{-1}	−4.62	4162
	0.1	1.71×10^{-21}	2.78	17001	1.21×10^{-1}	−4.73	3913
	0.025	5.02×10^{-21}	2.66	17317	2.50×10^{-2}	−4.72	3749
	0.01	1.98×10^{-21}	2.77	17123	1.02×10^{-2}	−4.73	3654
	0	2.17×10^{-17}	1.67	20987	9.67×10^{-21}	2.54	17226

[a] $k(T) = A\,T^B \exp(-C/T) + D\,T^E \exp(-F/T)$. Units are s^{-1} and cm^3 molecule^{-1} s^{-1} for unimolecular and bimolecular reactions, respectively. Temperature in Kelvin. [b] Ar diluent gas.

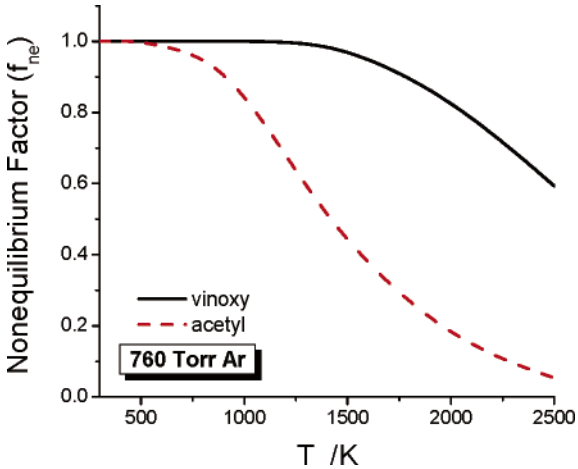

Figure 10. Calculated nonequilibrium (f_{ne}) factor for vinoxy and acetyl decomposition at 1 atm Ar.

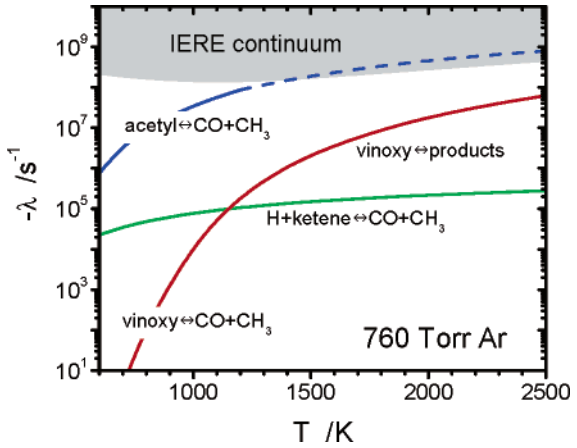

Figure 11. Chemically significant eigenvalues obtained from solving the master equation for the two-well problem at 1 atm Ar. Shaded region corresponds to the quasicontiuum of internal energy relaxation eigenvalues.

An indication of this condition is given by the nonequilibrium factor,[52] f_{ne}, defined as,

$$f_{ne}(T,P) = \frac{\left(\int_0^\infty c(E)\mathrm{d}E\right)^2}{\left(\int_0^\infty \frac{c(E)}{F(E)}c(E)\mathrm{d}E\right)^2} \qquad (5)$$

where *c(E)* is the steady-state distribution for a molecule dissociating irreversibly, and *F(E)* is the equilibrium distribution. The nonequilibrium factors for vinoxy and acetyl reactions are shown in Figure 10. When *c(E)* and *F(E)* are significantly different for states that are highly populated at equilibrium, f_{ne} will be less than unity, indicating that the rate of the chemical reaction is significant compared to that of the collisional process.

The chemically significant eigenvalues resulting from the two-well master equation are shown in Figure 11 for 1 atm of Ar bath gas. At low temperatures, the smallest (least negative) eigenvalue corresponds to the equilibration of vinoxy with bimolecular products. The next smallest eigenvalue equilibrates $H + CH_2CO$ with $CO + CH_3$, the bimolecular products, and

the largest corresponds to acetyl dissociating into CO + CH_3. At about 1500 K, the magnitude of the latter eigenvalue becomes comparable to those associated with internal energy relaxation through intermolecular collisions, depicted as the shaded region in Figure 11. This result indicates that acetyl equilibrates chemically with CH_3 + CO as part of the vibrational relaxation process. Under such conditions, the description of the reaction in terms of phenomenological rate coefficients becomes meaningless, although the very last bit of the reaction to take place can always be described in this way.[52]

Concluding Remarks

In this manuscript, we have studied the potential energy surface for the dissociation of vinoxy and acetyl radicals using high-level methods. Rate coefficients for the dissociation of these two radicals, and the related reverse reactions, were calculated using an RRKM/master equation model. Experimental data for the reverse reactions can be successfully predicted, without the need for ad hoc adjustments to the ab initio barriers or frequencies. Calculations for vinoxy decomposition agree with the experiments of Osborn et al.[13] in that the ketene channel is favored over the methyl one at photodissociation energies. This supports the conclusion of ref 13 that the $\tilde{B}(^2A'')$ state internally converts to the ground state before dissociation. Multireference configuration−interaction calculations indicate that there is a conical intersection between the $\tilde{X}(^2A'')$ and $\tilde{A}(^2A')$ surfaces at energies well below those of the transition states for isomerization and dissociation. At conditions relevant to combustion and atmospheric processes, thermal decomposition proceeds structurally via a 1,2-hydrogen shift to chemically activated acetyl, which immediately decomposes to CH_3 + CO. Note, however, that this is an elementary reaction in every sense of the word, which should be written as $CH_2CHO \leftrightarrow CH_3$ + CO.

Fits of all the rate coefficients considered in this paper are tabulated in Table 6 for temperatures between 200 and 2500 K and a range of pressures.

Acknowledgment. We thank D. Yarkony for sharing unpublished results with us. This work has been supported by the United States Department of Energy, Office of Basic Sciences, Division of Chemical Sciences, Geosciences, and Biosciences. Sandia is a multiprogram laboratory operated by Sandia Corporation, a Lockheed Martin Company, for the United States Department of Energy's National Nuclear Security Administration under contract DE-AC04-94AL85000. The work at Argonne was supported under DOE Contract Number W-31-109-ENG-38.

Supporting Information Available: Rovibrational properties of all species considered, calculated with the UB3LYP method. This material is available free of charge via the Internet at http://pubs.acs.org.

References and Notes

(1) Hidaka, Y.; Kimura, K.; Kawano, H. *Combust. Flame* **1994**, *99*, 18−28.

(2) Hranisavljevic, J.; Kumuran, S. S.; Michael, J. V. *Proc. Combust. Inst.* **1998**, 159−166.

(3) Irvine, W. M.; Friberg, P.; Kaifu, N.; Kagaguchi, K.; Kitamura, Y.; Matthews, H. E.; Minhh, Y.; Saito, S.; Ukita, N.; Yamamoto, S. *Astrophys. J.* **1989**, *342*, 871−875.

(4) Su, H. M.; Bersohn, R. *J. Chem. Phys.* **2001**, *115*, 217−224.

(5) Dimauro, L. F.; Heaven, M.; Miller, T. A. *J. Chem. Phys.* **1984**, *81*, 2339−2346.

(6) Endo, Y.; Saito, S.; Hirota, E. *J. Chem. Phys.* **1985**, *83*, 2026−2034.

(7) Brock, L. R.; Rohlfing, E. A. *J. Chem. Phys.* **1997**, *106*, 10048−10065.

(8) Alconcel, L. S.; Deyerl, H. J.; Zengin, V.; Continetti, R. E. *J. Phys. Chem. A* **1999**, *103*, 9190−9194.

(9) Nagai, H.; Carter, R. T.; Huber, J. R. *Chem. Phys. Lett.* **2000**, *331*, 425−432.

(10) Hansen, N.; Mader, H.; Temps, F. *J. Mol. Spectrosc.* **2001**, *209*, 278−279.

(11) Utkin, Y. G.; Han, J. X.; Sun, F. G.; Chen, H. B.; Scott, G.; Curl, R. F. *J. Chem. Phys.* **2003,** *118*, 10470−10476.

(12) Bowen, M. S.; Continetti, R. E. *J. Phys. Chem. A* **2004**, *108*, 7827−7831.

(13) Osborn, D.; Choi, H.; Mordaunt, D.; Bise, R.; Neumark, D.; Rohlfing, C. *J. Chem. Phys.* **1997**, *106*, 3049−3066.

(14) Mordaunt, D. H.; Osborn, D. L.; Neumark, D. M. *J. Chem. Phys.* **1998**, *108*, 2448−2457.

(15) Miller, J. L.; McCunn, L. R.; Krisch, M. J.; Butler, L. J.; Shu, J. *J. Chem. Phys.* **2004**, *121*, 1830−1838.

(16) Dupuis, M.; Wendoloski, J. J.; Lester, W. A. *J. Chem. Phys.* **1982**, *76*, 488−492.

(17) Yamaguchi, M. *Chem. Phys. Lett.* **1994**, *221*, 531−536.

(18) Matsika, S.; Yarkony, D. R. *J. Chem. Phys.* **2002**, *117*, 7198−7206.

(19) Lee, J.; Bozzelli, J. W. *Int. J. Chem. Kinet.* **2003**, *35*, 20−44.

(20) Colket, M. B.; Naegeli, D. W. Glassman, I. *Int. J. Chem. Kinet.* **1975**, *7*, 223−247.

(21) O'Neal, E.; Benson, S. W. *J. Chem. Phys.* **1962**, *36*, 2192−2203.

(22) Kerr, J. A.; Calvert, J. G. *J. Chem. Soc., Faraday Trans.* **1965**, *69*, 1022−1029.

(23) Frey, H.; Vinall, I. *Int. J. Chem. Kinet.* **1973**, *5*, 523−538.

(24) Watkins, K. W.; Word, W. W. *Int. J. Chem. Kinet.* **1974**, *6*, 855−873.

(25) Anastasi, C.; Maw, P. R. *J. Chem. Soc., Faraday Trans. 1* **1982**, *78*, 2423−2433.

(26) Baldwin, P. J.; Canosamas, C. E.; Frey, H. M.; Walsh, R. *Int. J. Chem. Kinet.* **1987**, *19*, 997−1013.

(27) Bencsura, A.; Knyazev, V. D.; Slagle, I. R.; Gutman, D.; Tsang, W. *Ber. Bunsen. Gesell. Phys. Chem.* **1992**, *96*, 1338−1347.

(28) Troe, J. *J. Phys. Chem. A* **2005**, *109*, 8320−8328.

(29) Miller, J. A.; Klippenstein, S. J. *Phys. Chem. Chem. Phys.* **2004**, *6*, 1192−1202.

(30) Becke, A.; *Phys. Rev. A* **1988**, *38*, 3098−3100.

(31) Stephens, P. J.; Devlin, F. J.; Chabalowski, C. F.; Frisch, M. J. *J. Phys. Chem.* **1994**, *98*, 11623−11627.

(32) Martin, J. M. L. *Chem. Phys. Lett.* **1996**, *259*, 669−678.

(33) Feller, D.; Dixon, D. A. *J. Chem. Phys.* **2001**, *115*, 3484−3496.

(34) Mayer, P. M.; Parkinson, C. J.; Smith, D. M.; Radom, L. *J. Chem. Phys.* **1998**, *108*, 604−615.

(35) Senosiain, J. P.; Klippenstein, S. J.; Miller, J. A. In preparation.

(36) Lee, T. J.; Taylor, P. R. *Int. Symp. Quantum Chem. Solid State Theory Mol. Dyn.* **1989**, *23*, 199−207.

(37) Lee, T. J.; Rendell, A. P.; Taylor, P. R. *J. Phys. Chem.* **1990**, *94*, 5463−5468.

(38) Young, R. A.; Yarkony, D. R. *J. Chem. Phys.* **2005**, *123*, 084315.

(39) Frisch, M. J.; Trucks, G. W.; Schlegel, H. B.; Scuseria, G. E.; Robb, M. A.; Cheeseman, J. R.; Zakrzewski, V. G.; Montgomery, J. A., Jr.; Stratmann, R. E.; Burant, J. C.; Dapprich, S.; Millam, J. M.; Daniels, A. D.; Kudin, K. N.; Strain, M. C.; Farkas, O.; Tomasi, J.; Barone, V.; Cossi, M.; Cammi, R.; Mennucci, B.; Pomelli, C.; Adamo, C.; Clifford, S.; Ochterski, J.; Petersson, G. A.; Ayala, P. Y.; Cui, Q.; Morokuma, K.; Malick, D. K.; Rabuck, A. D.; Raghavachari, K.; Foresman, J. B.; Cioslowski, J.; Ortiz, J. V.; Stefanov, B. B.; Liu, G.; Liashenko, A.; Piskorz, P.; Komaromi, I.; Gomperts, R.; Martin, R. L.; Fox, D. J.; Keith, T.; Al-Laham, M. A.; Peng, C. Y.; Nanayakkara, A.; Gonzalez, C.; Challacombe, M.; Gill, P. M. W.; Johnson, B. G.; Chen, W.; Wong, M. W.; Andres, J. L.; Head-Gordon, M.; Replogle, E. S.; Pople, J. A. *Gaussian 98*, revision A.7; Gaussian, Inc.: Pittsburgh, PA, 1998.

(40) Werner, H.-J.; Knowles, P. J.; Amös, R. D.; Bernhardsson, A.; Berning, A.; Celani, P.; Cooper, D. L.; Deegan, M. J. O.; Doobbyn, A. J.; Eckert, F.; Hampel, C.; Hetzer, G.; Korona, T.; Lindh, R.; Lloyd, A. W.; McNicholas, S. J.; Manby, F. R.; Meyer, W.; Mura, M. E.; Nicklass, A.; Palmieri, P.; Pitzer, R.; Rauhut, G.; Schütz, M.; Schumann, U.; Stroll, H.; Stone, A. J.; Tarroni, R.; Thorsteinsson, T. *MOLPRO* is a package of ab initio programs, version 2002.1, 1998.

(41) Pitzer, K. S.; Gwinn, W. D. *J. Chem. Phys.* **1942**, *10*, 428−440.

(42) Senosiain, J. P.; Miller, J. A.; Klippenstein, S. J. *J. Phys. Chem. A* **2005**, *109*, 6045−6055.

(43) Poling, B. E.; Prausnitz, J. M.; O'Connell, J. P. *The Properties of Gases and Liquids*, 5th ed.; McGraw-Hill: New York, 2001.

(44) Michael, J. V.; Nava, D. F.; Payne, W. A.; Stief, L. J. *J. Chem. Phys.* **1979**, *70*, 5222−5227.

(45) Miller, J. A.; Klippenstein, S. J.; Robertson, S. H. *J. Phys. Chem. A* **2000**, *104*, 7525−7536. See also Miller, J. A.; Klippenstein, S. J.; Robertson, S. H. *J. Phys. Chem. A* **2000**, 104, 9806−9806 (correction).

(46) Klippenstein, S. J.; Miller, J. A. *J. Phys. Chem. A* **2002**, *106*, 9267−9277.

(47) Miller, J. A.; Klippenstein, S. J. *J. Phys. Chem. A* **2003**, *107*, 2680−2692.

(48) Klippenstein, S. J.; Wagner, A. F.; Dunbar, R. C.; Wardlaw, D. M.; Robertson, S. H.; Miller, J. A. *VARIFLEX*, version 1.13m, 2003.

(49) Miller, J. A.; Parrish, C.; Brown, N. J. *J. Phys. Chem.* **1986**, *90*, 3339−3345.

(50) Hahn, D. K.; Klippenstein, S. J.; Miller, J. A. *Faraday Discuss.* **2001**, *119*, 79−100.

(51) Miller, J. A.; Klippenstein, S. J.; Raffy, C. *J. Phys. Chem. A* **2002**, *106*, 4904−4913.

(52) Miller, J. A.; Klippenstein, S. J. *J. Phys. Chem. A* **2004**, *108*, 8296−8306. See also: Smith, S. C.; McEwan, M. J.; Gilbert, R. J. *J. Chem. Phys.* **1989**, *90*, 4265−4273.

(53) Klippenstein, S. J.; Miller, J. A. *J. Phys. Chem. A* **2005**, *109*, 4285−4295.

(54) Carr, R. W.; Gay, I. D.; Glass, G. P.; Niki, H. *J. Chem. Phys.* **1968**, *49*, 846−852.

(55) Slemr, F.; Warneck, P. *Ber. Bunsen. Gesell. Phys. Chem.* **1975**, *79*, 152−156.

(56) Frank, P.; Bhaskaran, K. A.; Just, T. *J. Phys. Chem.* **1986**, *90*, 2226−2231.

(57) Parkes, D. A. *Chem. Phys. Lett.* **1981**, *77*, 527−532.

(58) Baulch, D. L.; Cobos, C. J.; Cox, R. A.; Frank, P.; Hayman, G.; Just, T.; Kerr, J. A.; Murrells, T.; Pilling, M. J.; Troe, J.; Walker, R. W.; Warnatz, J. *J. Phys. Chem. Ref. Data* **1994**, *23*, 847−1033.

(59) Peña-Gallego, A.; Martínez-Núñez, E.; Vázquez, S. A. *J. Chem. Phys.* **1999**, *110*, 11323−11334.